

pubs.acs.org/JPCC Article

Hierarchical Self-Assembly and Chemical Imaging of Nanoscale Domains in Polymer Blend Thin Films

Published as part of The Journal of Physical Chemistry virtual special issue "Nanophotonics for Chemical Imaging and Spectroscopy".

Tefera E. Tesema, Ross McFarland-Porter, Epherem Zerai, John Grey, and Terefe G. Habteyes*



Cite This: J. Phys. Chem. C 2022, 126, 7764–7772



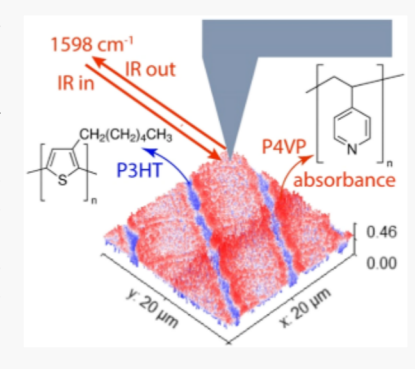
ACCESS

III Metrics & More

Article Recommendations

Supporting Information

ABSTRACT: Self-assembly of polymers driven by intermolecular and intramolecular interactions leads to rich structural variations in thin films of polymer blends. In this work, ordering of poly(3-hexylthiophene-2,5-diyl) (P3HT) to form nanoparticles (NPs) and the self-assembly pattern of the NPs in poly(4-vinylpyridine) (P4VP) matrix are revealed by using scattering-type scanning near-field optical microscopy (s-SNOM). The P3HT NPs are formed spontaneously when the P3HT/P4VP/chloroform solution is spin-cast on unpatterned silicon wafer at room temperature. We find that the P3HT NPs organize within the P4VP matrix forming continuous stripes along the parallel striations, depending on the solution composition and spin-coating angular speed. The spacing between the parallel P3HT stripes that runs along the center of the ridges varies from sample to sample within 4–12 μ m, whereas the width of the P3HT stripes confined within the ridges ranges from 0.2 to 1.1 μ m as determined from the s-SNOM infrared phase contrast. The sizes of the P3HT NPs range from 5 to over 100 nm depending on the composition of the blend as



determined by using an atomic force microscope after selectively dissolving the P4VP matrix. The smallest size observed in our experiment is significantly smaller than the smallest diameter (larger than 20 nm) reported in the literature. The results presented here show that interaction between immiscible polymers during solvent evaporation can be manipulated to control hierarchical self-assembly from molecular ordering to mesoscale dimensions, and high-resolution chemical imaging is necessary to resolve nanoscale domains so that solution processes can be optimized.

1. INTRODUCTION

Self-assembly of polymers (e.g., organic semiconductors) on unpatterned substrates through solvent evaporation is the simplest and cheapest route for fabricating organic electronics such as light-emitting diodes¹ and photovoltaics.^{2–4} It is also a natural and convenient procedure for fundamental studies of rich intermolecular interactions that may lead to hierarchical molecular ordering and intricate pattern formation. The morphology of the organic film depends on the processes that the thin film of solution undergoes from the time the solution is applied on the surface to postprocessing after the solvent evaporation is complete. Enhanced solvent evaporation at liquid-air interface induces temperature and concentration gradients, resulting in capillary forces and convection due to variation of surface tension (γ) from the surface to the subsurface. 5,6 For a liquid thin film that is continuously thinning during evaporation, the surface tension difference due to concentration gradient (∇C) at the surface is more dominant than the thermocapillary driving force.^{5,6} The convection driven by concentration gradient is characterized by Marangoni number (M) that depends on film height (H), solution viscosity (η) , and diffusion coefficient (D) as follows.

$$M = \frac{\left(\frac{\partial \gamma}{\partial C}\right) H^2 \nabla C}{\eta D} \tag{1}$$

In addition to the local interfacial tensions and other solution parameters, the morphology of the film will depend on the turbulence and other physical processes during the solvent evaporation. For example, a natural solvent evaporation from a drop-casted solution results in accumulation of solutes at the periphery of the film due to enhanced evaporation close to the pinning point that induces outward capillary flow. This process is commonly known as a "coffee-ring" effect. It has also been reported that controlling the evaporation in confined geometry can generate concentric rings of nonvolatile solutes due to stick—slip receding motion of the edge of the droplet. Spin-coating is a common technique used for

Received: February 22, 2022 Revised: April 12, 2022 Published: April 25, 2022





making a thin film of a mixture of two or more polymers from a common solvent for polymer-based optoelectronic devices such as light-emitting diodes, 12,13 field-effect transistor, 14,15 and organic semiconductor photovoltaics. $^{16-21}$ Phase separation in organic thin films prepared by spin-coating procedure is usually explained in terms of the Marangoni instability. In addition to rapid solvent evaporation, the spin-coating process exerts outward radial flow of solution due to centrifugal force. 5,11 Assuming a uniform surface coating, the final film thickness (h) can be expressed as 5

$$h = \frac{K}{\sqrt{\omega}} \left(\frac{3\eta}{2\rho} \frac{s^3}{1-s} \right)^{1/3} \tag{2}$$

where ω is the angular speed of the spin-coater, ρ is the density of the solution, s is fraction of the solute content in the solution, and K is a proportionality constant that depends on the air flow in the environment. In most cases, spin-casting of a solution generates thin films that consist of nanoscale domains with irregular shapes randomly distributed throughout the substrate. Deviation from thickness uniformity in spin-coated film can originate from the influence of air current on the localization of interfacial tensions across the solution surface that leads to Marangoni instability depending on the volatility of the solvent, 16,17 viscosity, diffusion, and substrate functionalization. 18

The Marangoni instability can be harnessed to generate regular patterns such as parallel ridges, where both thickness and composition can be modulated. For example, depending on the solution composition, alternating parallel stripes of polystyrene (PS) and poly(vinylpyrrolidone) (PVP) have been observed in the PS/PVP blend thin film spin-casted from a chloroform solution on unpatterned substrates. Similarly, a periodic pattern of stripes with microscale pore size has been observed on spin-casted thin films of PS and poly(ethylene glycol) due to convection during radial flow, solvent evaporation, and phase separation. 19 In more recent studies, holes aligned along the centrifugal force have been observed upon spin-casting poly(4-vinylpyridine) (P4VP) film on preformed PS thin film²⁰ as well as in PS film spin-casted on poly(methyl methacrylate) film^{6,21} due to directional dewetting effect and interfacial instability.^{22,23} In the studies reported to date, the domain sizes are on the order of several micrometers, and the periodicity of the patterns is usually larger than 30 μ m. In addition, the chemical composition of the domains has not been resolved by using optical microscopy with relevant spatial resolution.^{6,19-21} Wu et al. used an infrared beam size of $\sim 10 \, \mu \text{m}$ to determine that the alternating stripes in PS/PVP blend film have different chemical composition indicating large-scale phase separation. However, this resolution is far from satisfactory, particularly considering that the appropriate spatial resolution for characterizing organic electronic materials should be comparable to the exciton diffusion length, which is less than 20 nm. 24,25

In this work, hierarchical self-assembly of nanoscale domains in spin-casted thin films of P3HT and P4VP polymer blend is investigated by using a scattering-type scanning near-field optical microscope (s-SNOM) that achieves spatial resolution on the order of 10 nm independent of excitation wavelength. The choice of P3HT is motivated by its use as prototypical organic semiconductor in organic electronic research. In addition, experimental studies indicate that interfacing P3HT thin film with P4VP can result in significant

increase of electrical conductivity possibly due to contribution of the P4VP permanent dipole orientation to the interfacial electrical property.³⁰ In our recent study, pure P4VP thin film with thickness gradient have been used as a model system to study the molecular sensitivity of s-SNOM vibrational infrared (IR) imaging by probing the P4VP ring vibration mode frequency.³¹ Here, the hierarchical self-assembly in the P3HT/ P4VP blend is studied by targeting the P4VP component in the binary system. The s-SNOM chemical imaging has revealed stripes of P3HT with width as small as 200 nm arranged within the P4VP-rich parallel ridges. The spacing between the parallel P3HT stripes varies from sample to sample within 4–12 μ m, which is significantly smaller than expected for wavelength of striation on unpatterned substrates. Further analysis reveals that the P3HT domains consist of NPs that are formed spontaneously during spin-casting and solvent evaporation on the substrate at room temperature. The diameter of the NPs ranges from 5 to over 100 nm depending on the P3HT concentration in the solution. The P3HT NPs organize within the P4VP matrix of striations to form continuous stripes depending on the solution composition. Overall, the results presented here show that s-SNOM IR vibrational imaging reveals nanoscale chemical domains so that solution processes can be optimized to achieve hierarchical self-assembly.

2. EXPERIMENTAL METHODS

Sample Preparation. Regionegular P3HT (molecular weight $M_{\rm w}=50000-75000$) and P4VP ($M_{\rm w}=60000$) were obtained from Sigma-Aldrich. Solutions of P3HT and P4VP are prepared separately (Figure 1) in common chloroform

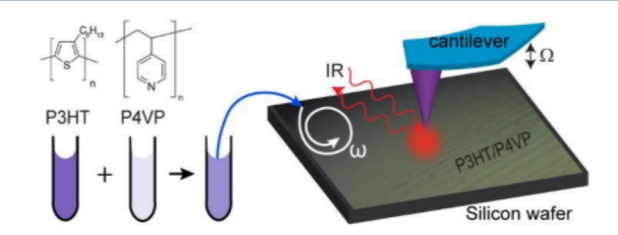


Figure 1. Schematic showing the sample preparation and a simplified s-SNOM setup. Solutions of P3HT and P4VP are separately prepared in chloroform and mixed. The blended solution is then spin-casted on a silicon wafer at spin-coating speed of ω . The dried film is studied by using s-SNOM at IR excitation wavelengths to resolve nanoscale chemical domains. Ω is the cantilever oscillation frequency.

solvent at equal concentration of 2.6 mg/mL. A solution that contains both polymers at different mass (m) fraction, $f = m_{P3HT}/(m_{P3HT} + m_{P4VP})$, is then prepared by taking appropriate volume from each polymer solution to make a 100 μ L of the blend solution at constant total polymer concentration of 2.6 mg/mL. The mass fractions used in this experiment range from f = 0.02 to 0.5. Thin films of P3HT/P4VP blends of varying composition is prepared by spin-coating 5 μ L of the blend solution on a silicon wafer at room temperature at an angular speed of $\omega = 1500-7000$ rpm by using the spin-coating system of Laurell Technologies Corporation (Model WS-650MZ-23NPP) that has internal nitrogen gas flow to purge the air above the sample. The spin-coater is operated in dynamic mode, where the blend solution is applied on the substrate after the ramping is complete and the set speed is attained.

Chemical Imaging. Chemical phase separation and nanoscale domains in the P3HT/P4PV blend are studied by

using s-SNOM, which is based on the integrated atomic force microscope (AFM) and near-field microscope system of Neaspec GmbH. The schematic in Figure 1 shows a simplified layout of the s-SNOM setup. In the past, we have used a similar s-SNOM system for imaging plasmon modes on individual^{32,33} and coupled nanostructures²⁶ by using visible excitation wavelengths, and the technical details are the same except that the IR laser source (quantum cascade laser, QCL) is used in the present experiment similar to our most recent report.³¹ The AFM is operated in tapping mode with a dithering amplitude of ~80 nm at cantilever's natural resonance oscillation frequency of $\Omega \sim 250$ kHz. The QCL (MIRCat-1200, Daylight Solution) system generates linearly polarized IR radiation with tunable frequency. The IR laser is focused by using a parabolic mirror (NA = 0.46) at the tipsample interface at a grazing incidence angle of 30° with respect to the sample plane. The IR scattering from the tipsample junction is detected by using HgCdTe photodiodes (Kolmar Technologies, Inc.) at liquid nitrogen temperature implementing a pseudo-heterodyne interferometric detection principle such that both IR amplitude and phase are recorded simultaneous with the AFM topographic image.³⁴ The detector's output is demodulated at higher harmonics of the cantilever oscillation frequency, and the results at 3 Ω are presented and discussed. The chemical heterogeneity is revealed by recording the IR image at 1598 cm⁻¹ that matches the peak frequency of the P4VP ring vibrational mode.³¹ The IR contrast in the on-resonance images are compared to that of the off-resonance images obtained at laser frequency of 1570 cm⁻¹ that does not have significant overlap with any of the vibrational frequencies of the P4VP or P3HT components as illustrated in Figure S1. Ideally, the distribution of the P3HT domains should be obtained by recording the s-SNOM image at the corresponding vibrational frequencies (e.g., at 1456 cm⁻¹, Figure S1) similar to the recent study by Goikoetxea et al. 35 Unfortunately, all the vibrational frequencies of the P3HT component are outside the tunability range of our QCL. Nevertheless, a negative correlation between the topographic height and IR phase must indicate the P3HT domain as there are only two components in the blend that is considered in this study.

3. RESULTS

The results in Figure 2 illustrate our approach for resolving nanoscale domains in polymer blend thin films using s-SNOM chemical imaging. The IR phase contrast obtained at the resonance of the P4VP vibrational absorption transition reveals the distribution of the components with high spatial resolution in a relatively large scan area (Figure 2b). On the other hand, a smooth and featureless optical phase image is obtained at the off-resonance laser line of 1570 cm⁻¹ (Figure 2c) that has no overlap with any of the P4VP or the P3HT vibrational bands (Figure S1). The difference in the details of the chemical contrast at on- and off-resonance excitation conditions can be observed by comparing the line profiles in Figures 2d,e, where the on-resonance IR phase exhibits drastic fluctuation (blue line) corresponding to lateral chemical heterogeneity compared to the relatively smooth green line at off-resonance excitation frequency. Upon comparison of the on-resonance variation in the IR phase (blue line, Figure 2e) to the height variation (Figure 2d), it is clear that the chemical identity of the nanoscale domains identified in the IR image is not obvious in the topographic image (Figure 2a). Additional

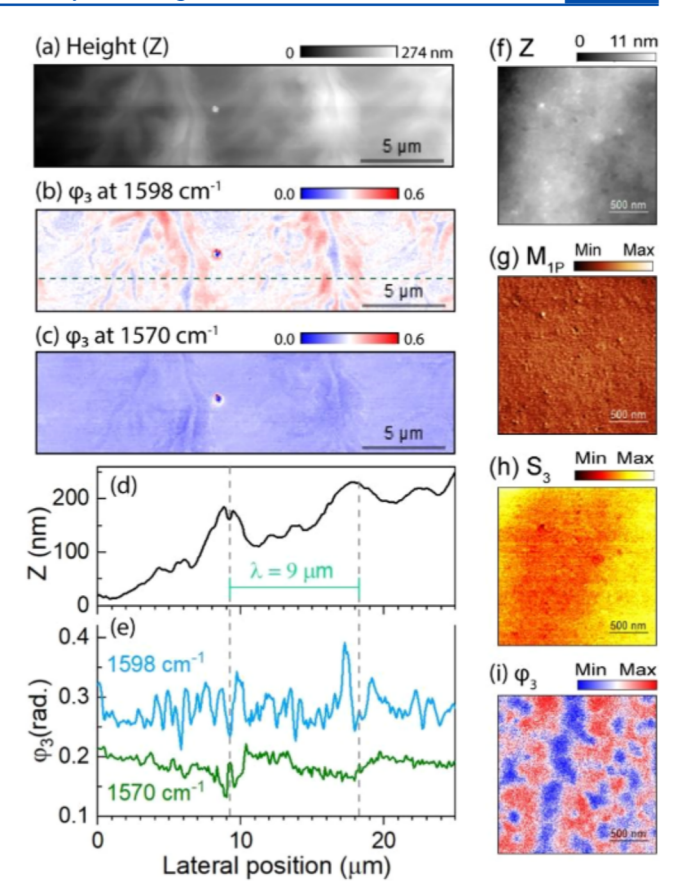


Figure 2. IR s-SNOM image of P3HT/P4VP blend with f=0.5 spin-coated at 5000 rpm onto Si substrate. (a) AFM topography, (b) IR near-field phase at on-resonance excitation, and (c) IR near-field phase at off-resonance excitation. (d) Line profile of topography and (e) line profiles of IR near-field phase at on-resonance (blue line) and off-resonance (green line) excitation frequencies. (f—i) Small area scan showing AFM topography (f), mechanical phase (g), IR near-field amplitude (h), and IR near-field phase (i).

details of contrast can be observed in the mechanical force amplitude and phase images (Figure S2) but not with the level of details and chemical specificity observed in the IR phase image.

The force and IR images in Figures 2f-i are recorded simultaneously by scanning a relatively small area. Although the morphology appears uniform in the AFM height/phase images (Figures 2f,g), variation of chemical domains at the nanoscale is observed in the IR phase image (Figure 2i). The phase shift is related to the imaginary part of the dielectric function, and therefore it provides direct chemical contrast due to absorption differences between the components. That is, in the IR phase image (Figure 2i), a higher phase shift is observed when the probe interacts with the P4VP component that has vibrational absorption resonance at the excitation frequency, resulting in the visualization of the P4VP domains (red regions) and P3HT domains (blue region) in real space. On the other hand, the scattering amplitude is related to the real part of the dielectric function,³¹ and the signal is dominated by the high reflectivity of the substrate (silicon). As a result, the scattering amplitude decreases with increasing overall thickness of the polymer blend, resulting in darker regions at high polymer thickness as displayed in Figure 2h. We will use the complementary information to investigate the hierarchical self-

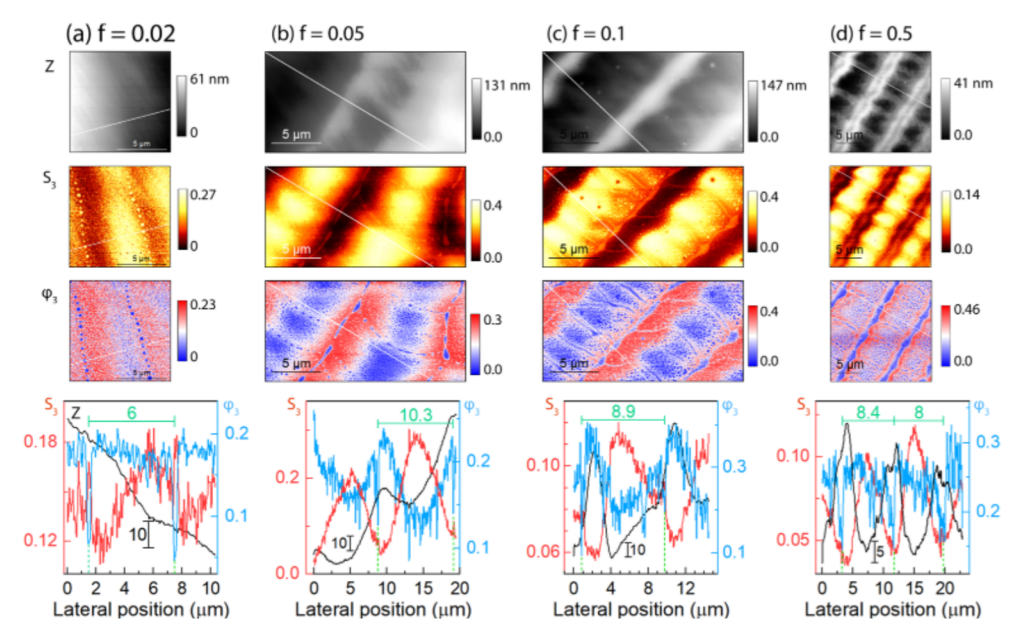


Figure 3. Effect of composition on hierarchical self-assembly at fixed spin-coating speed of 5000 rpm. At f = 0.02 (a) and f = 0.05 (b), hole arrays and disconnected stripes, respectively, of P3HT are observed within the P4VP ridges. At f = 0.1 (c), the ridges are more defined, the stripes are mostly connected, the spacing is reduced to ~9 μ m, and bridges that connect the ridges start to form. At f = 0.5 (d), the stripes are fully connected. The line profiles (bottom panels) are along the diagonal white lines on the images (the vertical scale bar corresponds to the black line, topographic height). The spacing (green scale) is measured by using adjacent P3HT stripes (dips in the IR phase) as reference points.

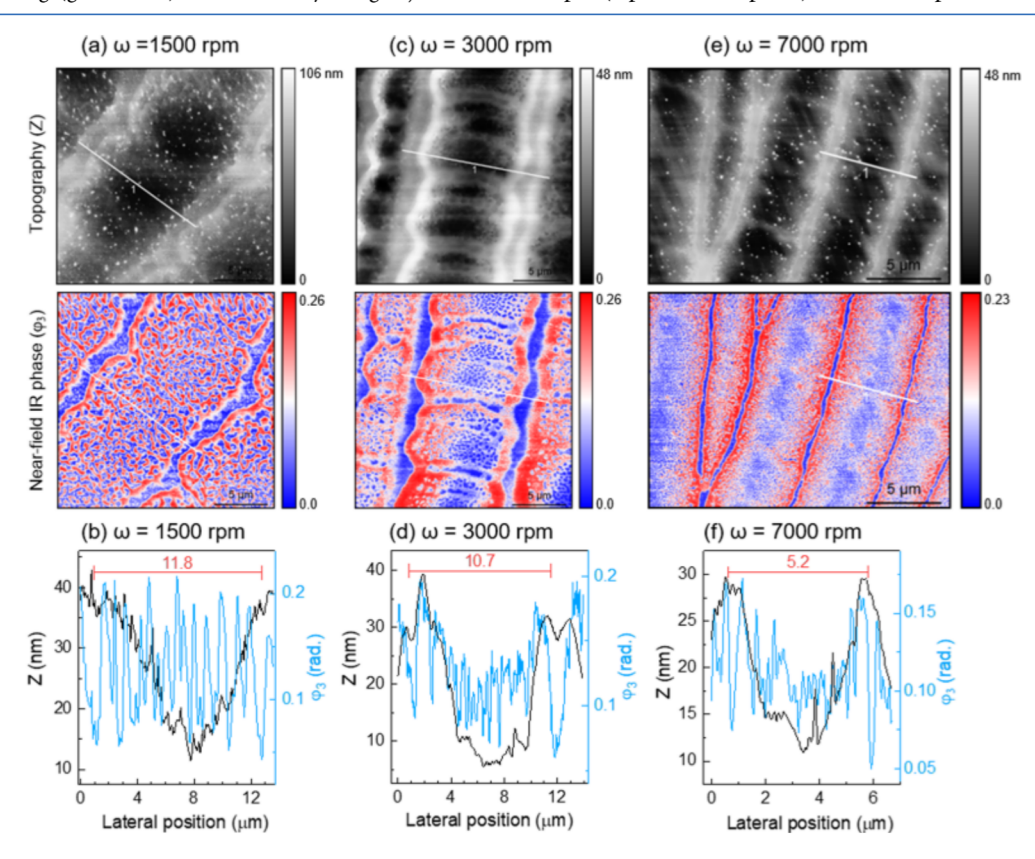


Figure 4. Effect of spin-coating speed on the striation pattern in the P3HT/P4VP blend film at fixed composition of 0.5. AFM topography (first row) and IR near-field phase (second row) and the corresponding line profiles across the vertical white lines on the images for ω = 1500 rpm (a, b), ω = 3000 rpm (c, d), and ω = 5000 rpm (e, f).

assembly of nanoscale domains in the P3HT/P4VP blend as discussed next.

The morphology and thickness of the film vary radially, changing from random cellular structures at the center of the

film to a somewhat regular pattern of parallel striations going outward (see bright-field optical images in Figure S3). Analysis of the film structures for the pure components indicates that the striation pattern is mainly characteristic of the P4VP

component (Figure S4), which is less soluble in chloroform than P3HT. The assembly of the P3HT domains within the P4VP matrix depends sensitively on the composition of the blend as illustrated in Figure 3 at a fixed spin-coating speed of 5000 rpm. At f = 0.02, linearly arranged holes have been observed as revealed in the IR amplitude and phase images (Figure 3a). In general, the linear alignment of the hole arrays is in agreement with past observations in bilayer polymer films^{20,21} and can be attributed to dewetting effects resulting from the interplay between the interfacial tensions at the substrate and air interfaces.²³ However, the spacing between the parallel arrays (see line profile in Figure 3a, bottom panel) is significantly smaller than reported values (>30 μ m).²¹ As the P3HT mass fraction increases, the hole arrays appears to connect (Figures 3b-d). The high points in the topography correspond to dark regions in the IR scattering amplitude (second row in Figure 3), while the fine details due to variation in the chemical domains are revealed in the IR phase images (third row). For more quantitative analysis, the line profiles perpendicular to the parallel striations (across the diagonal white lines on the images) are plotted in Figure 3 (bottom panels), where generally a negative correlation is observed between the topographic height (black lines) and the IR scattering amplitude (red lines). Comparing the IR phase contrast (blue lines) to the topographic height (black line), it can be seen that the ridges are P4VP-rich. The accumulation of the P4VP along the ridges can be attributed to the fact that P4VP is less soluble than P3HT in chloroform, which can lead to faster rate of solvent evaporation and rapid solidification of the P4VP domain.³⁶ The phase contrast also reveals nanoscale domains of P3HT along the ridges as indicated by the blue regions in the images (Figure 3, second row). At f = 0.05(Figure 3b) disconnected stripes of P3HT domains are observed along the P4VP ridges. Using the P3HT domains within the ridges as reference points, we estimated a periodicity of $\lambda \sim 10 \ \mu \text{m}$. At f = 0.1 (Figure 3c), the ridges are more defined; the P3HT domains within the ridges are mostly connected, and bridges that connect the ridges start to form. At f = 0.5 (Figure 3d), the hierarchical assembly is well-defined with the P3HT domains within the ridges forming long stripes. Interestingly, the overall microstructures of the height image in Figure 3d have some resemblance with the popular microstructures in butterfly wings.³⁷ Considering all the composition variation, the striation wavelength (defined as the distance between adjacent P3HT stripes) ranges from 6 to 10 μ m as shown on the line profile plots (bottom panels in Figure 3) with no obvious correlation to the P3HT mass fraction. Overall, the periodicity in the P3HT/P4VP blend remains reliably much smaller than the reported values for other blends that produces periodicity larger than 30 μ m⁵ as illustrated, for example, in PS/poly(vinylpyrrolidone)⁶ and PS/PMMA²¹ blends.

The effect of spin-coating speed (ω) on the film morphology is illustrated in Figure 4 at fixed P3HT mass fraction of 0.5. Both the width of the ridges and the periodicity of the striation pattern decrease with increasing ω as can be seen in the images and line profiles in Figure 4. Overall, the periodicity of the striations remains short compared to past reports, but variations of λ have been observed upon repeating the sample preparation at nominally the same conditions. For example, $\lambda \approx 9 \ \mu \text{m}$ in Figure 3c and $\lambda \approx 4 \ \mu \text{m}$ in Figure S5 have been obtained for samples prepared on different days at the same composition (f = 0.1) and the same spin-coating speed of 5000

rpm. However, within the same sample, the spacing between successive ridges is reproducible within 0.5 μ m as the λ values in Figure 3d and Figure S5 indicate. The width of the ridges is estimated from the AFM force image (it can also be estimated from the s-SNOM scattering amplitude), whereas the dimension of the chemical domains can be estimated from the s-SNOM IR phase images as illustrated in Figures S6 and S7. The width of the ridge varies from about 4 to 1.5 μ m depending on the sample preparation, while the width of the P3HT stripes that run along the ridges ranges from about 0.2 to 1 μ m.

The P3HT stripes in the s-SNOM IR phase images should not be confused with a continuous and long P3HT fiber. It is difficult to confirm a nanometer and subnanometer lateral material continuity in the IR phase as nanostructures of the same chemical identity can aggregate linearly to create the appearance of extended P3HT domain. Close observation of the AFM topographic images reveals that the P3HT domains consist of discrete P3HT NPs that are self-assembled hierarchically (see the enlarged AFM image in Figure S8). Clear evidence for the formation of the P3HT NPs is obtained by scanning different regions on different samples. For some samples, a monolayer of P3HT NPs has been observed in certain regions due to large-scale phase separation, where the striation pattern is absent as shown in Figure 5a. The chemical

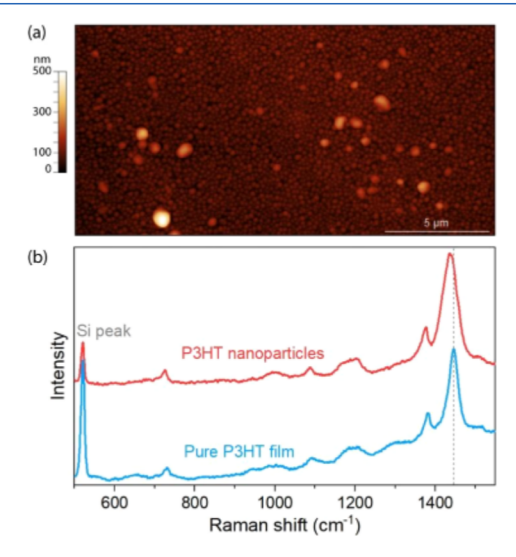


Figure 5. (a) Close-packed monolayer of P3HT nanoparticles formed spontaneously during the spin-coating and solvent evaporation (f = 0.3 and $\omega = 500$ rpm). (b) Raman spectrum of P3HT nanoparticles (red line) compared to that of pure P3HT film (blue line).

identity of the nanoparticles is confirmed by using Raman spectroscopy (Figure 5b). Comparison of the Raman spectra of the P3HT NPs to that of pure P3HT film indicates about a 15 cm⁻¹ downshift, which is in agreement with past observations of similar shift due to interchain interaction in H-type aggregates.³⁸

Selective dissolution confirms that the P3HT NPs are formed at all mass fractions considered. That is, AFM imaging of the film after selectively dissolving the P4VP component (by soaking the blend film in ethanol, a good solvent for P4VP, for about 30 s) exposes the P3HT NPs. Examples of the P3HT NPs revealed through the selective dissolution are shown in Figure S9 for f = 0.05. The size of the NPs increases with

concentration, consistent with past observations.³⁹ For example, at f = 0.3 (Figure 5), the diameter of the NPs is about 80 nm as estimated from the AFM height measurement. On the other hand, for f = 0.05, the NPs have diameters as small as 5 nm, which is significantly smaller than the smallest size reported in the literature by using other methods.⁴⁰ In general, the P3HT NPs are formed at all composition and spin-coating speed in dynamic modes. Overall, the observation of the NPs and their distribution within the P4VP matrix indicate that P3HT ordering and crystallization may take place rapidly at the beginning of the spin-coating and solvent evaporation processes.

4. DISCUSSION

The results presented in this work show the hierarchical selfassembly of P3HT polymer within striation patterns of the P3HT/P4VP blend film formed by spin-casting on unpatterned silicon wafer. The periodicity of the striation is significantly shorter than the periodicity observed in past experiments, where the film structure is dictated by Marangoni instability. The length scale is also smaller than the corresponding wavelength in other sample varieties. For example, in PS/AuNPs blend drop-casted from chloroform solvent, radially aligned microchannels have been formed spontaneously with λ ranging from 12 to 35 μ m. ⁴¹ In the sol– gel-derived films of silica-poly(vinylpyrrolidone) prepared by using a dip-coating process, the spacing between the adjacent linearly arranged parallel striations is larger than 100 μ m. Similarly, striations in films prepared by casting polymer solution at a tilt angle has periodicity larger than 30 μ m, ⁴³ while spin-coating of SiO₂ and TiOx sol-gel mixture solution produces striations with $\lambda > 50 \mu m.^{44}$

The more striking observation in the P3HT/P4VP blend is the observation of the P3HT stripes with width as narrow as 200 nm within the P4VP-rich ridges. This is in contrast to the expectation of alternating composition based on past observation in PS/PVP blend⁶ due to large-scale phase separation considering that P3HT and P4VP can be considered immiscible components. The formation of the P3HT domains within the P4VP ridges can be attributed to the formation of the P3HT NPs at the beginning of the spincoating and solvent evaporation processes as illustrated by the schematic in Figure 6. Considering that chloroform is not a good solvent for P4VP, the solvent molecules will be lost from the P4VP region at a faster rate, inducing concentration and surface tension gradient that leads to diffusion and accumulation of P4VP to form the parallel ridges. However, if the P3HT NPs are formed before the viscosity of the solvent is preventing the flow of the suspension, they can be found everywhere within the fluid. As the solvent evaporation is progressing, the P4VP component can solidify around the aggregates of the P3HT NPs that can then be trapped within the P4VP side walls (Figure 6, bottom panel). In this regard, the process during the spin-casting of the P3HT/P4VP blend has similarity to the metal nanoparticle aggregation pattern along striations during spin-casting of nanoparticle/polymer mixture, 41,45 except that in the current case the P3HT NPs are formed during the spin-coating process.

The absorption spectra of the P3HT/P4VP/chloroform solution and that of the film prepared at different solution compositions are compared in Figure 7. The results show that the absorption wavelengths of the film have red-shifted significantly compared to that of the solution, which is in

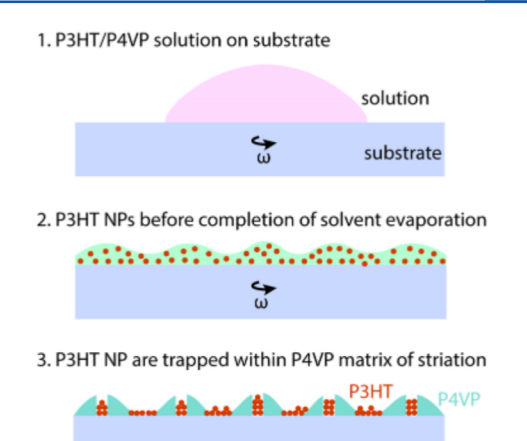


Figure 6. Possible sequence of physical processes during spin-casting and solvent evaporation. The P3HT/P4VP/chloroform solution is applied on the substrate after the spin-coater has attained the desired speed. We propose that the P3HT NPs are formed at the beginning of spinning before solvent evaporation is complete. As the solvent evaporation continues, the P3HT NPs are trapped within the P4VP matrix.

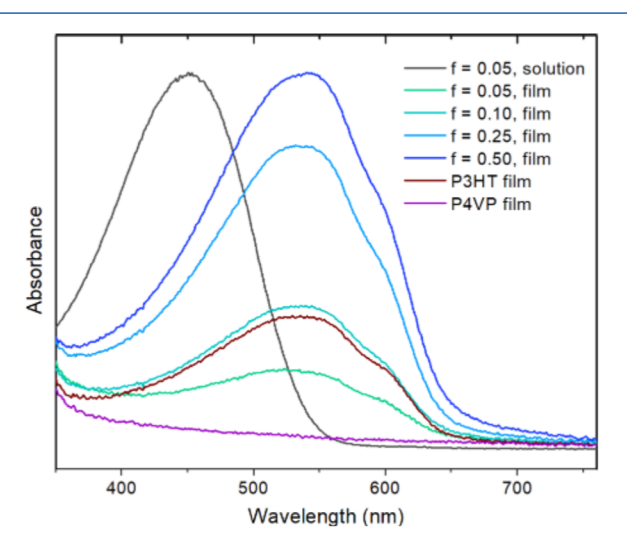


Figure 7. Absorption spectrum of the P3HT/P4VP/chloroform solution (black line) and the film at different mass fractions of P3HT as labeled. The absorption for the pure P3HT (brown line) is obtained from a film prepared by using a solution with P3HT concentration equivalent to that in the f=0.1 blend. The purple line indicates that P4VP film is transparent in this spectral window. The rise below 400 nm is due to background in the cover glass used to support the film.

agreement with past reports, and it is attributed to the P3HT ordering and interchain interaction in the nanoscale domains. In addition, close observation reveals that the spectra of the film is convolution of three bands (0-0, 0-1, 1) and a shoulder peak at ~ 605 nm), which is consistent with published spectra of P3HT NPs deposited on glass. We note that the spectral shape of the photoabsorption of the pure P3HT solution and the P3HT/P4VP blend solution are identical, confirming that the P3HT NPs are not formed in the solution. The absorption spectra shown by the purple line in Figure 7 indicate that pure P4VP film is transparent in the given window, and the optical density increases with increasing mass fraction of P3HT in the film. The spectra also show that

absorption of P3HT NPs in the P4VP matrix have similar absorption bands as that of the corresponding aggregates in pure P3HT film as can be seen comparing the cyan and brown lines in Figure 7. The similarity of the absorption bands is evidence for similar ordering of P3HT polymer chains regardless of the different morphologies of the nanoscale domains. However, determining the exact crystallinity within the P3HT NPs depending on size and processing condition requires future studies using X-ray spectroscopy.

It is interesting to note that for a given sample the spacing between adjacent ridges is reproducible within 0.5 μ m as mentioned above. This observation implies that the Marangoni instability inducing the striation has well-defined wavelengths. It has been reported that striation patterns do not form in films spin-cast in a closed system. The periodicity may be defined by the resultant effect of the flow of gas above the solution and the solution parameters. That is, a governing sinusoidal surface wave in the form of $h(x,t) = h(t) \sin(kx - \omega t)$ (where h(t) represents uniform film height that thins with time t, and k is the propagating wave vector) may define enhanced regions of solvent evaporation and surface tension localization at the beginning of the solvent evaporation process.

$$\frac{\Delta G_{\text{mix}}}{k_{\text{B}}T} = \chi \varphi_{\text{A}} \varphi_{\text{B}} + \frac{\varphi_{\text{A}}}{N_{\text{A}}} \ln(\varphi_{\text{A}}) + \frac{\varphi_{\text{B}}}{N_{\text{B}}} \ln(\varphi_{\text{B}})$$
(3)

where $k_{\rm B}$ is the Boltzmann constant and χ is the Flory–Huggins interaction parameter. According to this model, the mixing between A and B is thermodynamically favorable when $\Delta G_{\rm mix}$ is negative. In eq 3, the enthalpy of mixing (first term) is most likely positive, and the contribution of the entropy of mixing terms (the second and the third terms) is small, resulting in overall positive $\Delta G_{\rm mix}$ that favors phase separation. The tendency of P3HT to crystallize can further enhance the phase separation behavior. However, the fact that nanoscale domains of P3HT are distributed throughout the P4VP matrix indicates some level of P3HT–P4VP intermolecular interactions.

5. CONCLUSION

In conclusion, the hierarchical self-assembly of P3HT nanoscale domains within the P4VP matrix is revealed by using s-SNOM chemical imaging at infrared laser frequency tuned to the P4VP ring stretching vibrational absorption resonance. Parallel ridges that are occasionally connected with bridges are formed spontaneously upon spin-casting of the polymer blend on unpatterned substrate. The periodicity of the striations determined from the s-SNOM IR vibrational images is less than 12 μ m, which is significantly smaller than striation wavelengths observed in the past in thin films of different polymer components. The ridges consist of P3HT stripes with width as narrow as 200 nm supported by a P4VP wall on each side. Further analysis of the blend film reveals that the P3HT domains result from self-assembly of nanoparticles that form spontaneously during the spin-coating process. The smallest size of the NPs observed in this work is about 5 nm

(significantly smaller than previously achieved), which provides large surface area that may be important for device applications. Overall, the results presented here show that s-SNOM vibrational imaging reveals nanoscale chemical domains so that hierarchical self-assembly may be achieved by optimizing solution processes.

ASSOCIATED CONTENT

Supporting Information

The Supporting Information is available free of charge at https://pubs.acs.org/doi/10.1021/acs.jpcc.2c01289.

FTIR spectra of P3HT and P4VP (Figure S1); comparison of force and IR scan images (Figure S2); bright-field images of P3HT/P4VP thin film (Figure S3); topography and IR phase of pure P4VP film (Figure S4); periodicity in P3HT/P4VP blend film (Figure S5); width of the ridges and P3HT stripes within the ridges (Figure S6); observation of narrow P3HT stripes (Figure S7); topographic image showing P3HT nanoparticles (Figure S8); and topography of the P3HT NPs after dissolving the P4VP component (Figure S9) (PDF)

AUTHOR INFORMATION

Corresponding Author

Terefe G. Habteyes — Department of Chemistry and Chemical Biology and Center for High Technology Materials, University of New Mexico, Albuquerque, New Mexico 87131, United States; oorcid.org/0000-0001-5978-6464; Email: habteyes@unm.edu

Authors

Tefera E. Tesema — Department of Chemistry and Chemical Biology and Center for High Technology Materials, University of New Mexico, Albuquerque, New Mexico 87131, United States; Occid.org/0000-0003-0431-8705

Ross McFarland-Porter — Department of Chemistry and Chemical Biology and Center for High Technology Materials, University of New Mexico, Albuquerque, New Mexico 87131, United States

Epherem Zerai — Center for High Technology Materials, University of New Mexico, Albuquerque, New Mexico 87131, United States

John Grey — Department of Chemistry and Chemical Biology, University of New Mexico, Albuquerque, New Mexico 87131, United States; Oorcid.org/0000-0001-7307-8894

Complete contact information is available at: https://pubs.acs.org/10.1021/acs.jpcc.2c01289

Notes

The authors declare no competing financial interest.

ACKNOWLEDGMENTS

This research has been supported by the U.S. National Science Foundation (Grant No. 1651478). T.E.T. has been supported by AFOSR Grant No. FA9550-19-1-0163 during the final phase of experiments and manuscript preparation.

REFERENCES

(1) Yim, K.-H.; Doherty, W. J.; Salaneck, W. R.; Murphy, C. E.; Friend, R. H.; Kim, J.-S. Phase-Separated Thin Film Structures for

- Efficient Polymer Blend Light-Emitting Diodes. *Nano Lett.* **2010**, *10*, 385–392.
- (2) Campbell, A. R.; Hodgkiss, J. M.; Westenhoff, S.; Howard, I. A.; Marsh, R. A.; McNeill, C. R.; Friend, R. H.; Greenham, N. C. Low-Temperature Control of Nanoscale Morphology for High Performance Polymer Photovoltaics. *Nano Lett.* **2008**, *8*, 3942–3947.
- (3) McNeill, C. R.; Halls, J. J. M.; Wilson, R.; Whiting, G. L.; Berkebile, S.; Ramsey, M. G.; Friend, R. H.; Greenham, N. C. Efficient Polythiophene/Polyfluorene Copolymer Bulk Heterojunction Photovoltaic Devices: Device Physics and Annealing Effects. *Adv. Funct. Mater.* **2008**, *18*, 2309–2321.
- (4) McNeill, C. R.; Westenhoff, S.; Groves, C.; Friend, R. H.; Greenham, N. C. Influence of Nanoscale Phase Separation on the Charge Generation Dynamics and Photovoltaic Performance of Conjugated Polymer Blends: Balancing Charge Generation and Separation. *J. Phys. Chem. C* 2007, 111, 19153—19160.
- (5) Birnie, D. P. Rational Solvent Selection Strategies to Combat Striation Formation during Spin Coating of Thin Films. *J. Mater. Res.* **2001**, *16*, 1145–1154.
- (6) Wu, K.-H.; Lu, S.-Y.; Chen, H.-L. Formation of Parallel Strips in Thin Films of Polystyrene/Poly(Vinyl Pyrrolidone) Blends via Spin Coating on Unpatterned Substrates. *Langmuir* **2006**, *22*, 8029–8035.
- (7) Deegan, R. D.; Bakajin, O.; Dupont, T. F.; Huber, G.; Nagel, S. R.; Witten, T. A. Capillary Flow as the Cause of Ring Stains from Dried Liquid Drops. *Nature*. **1997**, *389*, 827–829.
- (8) Jeon, J.; Tan, A. T. L.; Lee, J.; Park, J. E.; Won, S.; Kim, S.; Bedewy, M.; Go, J.; Kim, J. K.; Hart, A. J.; et al. High-Speed Production of Crystalline Semiconducting Polymer Line Arrays by Meniscus Oscillation Self-Assembly. ACS Nano 2020, 14, 17254–17261.
- (9) Park, W. I.; Kim, D.-H.; Jung, J.; Hong, S. W.; Lin, Z.; Byun, M. Spatially Ordered Poly(3-Hexylthiophene) Fibril Nanostructures via Controlled Evaporative Self-Assembly. *Adv. Mater. Technol.* **2019**, *4*, 1800554.
- (10) Lin, Z.; Granick, S. Patterns Formed by Droplet Evaporation from a Restricted Geometry. *J. Am. Chem. Soc.* **2005**, *127*, 2816–2817.
- (11) Meyerhofer, D. Characteristics of Resist Films Produced by Spinning. *J. Appl. Phys.* **1978**, *49*, 3993–3997.
- (12) Chen, J.; Chen, Z.; Qu, Y.; Lu, G.; Ye, F.; Wang, S.; Lv, H.; Yang, X. Large Interfacial Area Enhances Electrical Conductivity of Poly(3-Hexylthiophene)/Insulating Polymer Blends. *RSC Adv.* **2015**, *5*, 1777–1784.
- (13) Wu, Y.; Peng, Y.; Bohra, H.; Zou, J.; Ranjan, V. D.; Zhang, Y.; Zhang, Q.; Wang, M. Photoconductive Micro/Nanoscale Interfaces of a Semiconducting Polymer for Wireless Stimulation of Neuron-Like Cells. ACS Appl. Mater. Interfaces 2019, 11, 4833–4841.
- (14) Hou, S.; Yu, J.; Zhuang, X.; Li, D.; Liu, Y.; Gao, Z.; Sun, T.; Wang, F.; Yu, X. Phase Separation of P3HT/PMMA Blend Film for Forming Semiconducting and Dielectric Layers in Organic Thin-Film Transistors for High-Sensitivity NO Detection. ACS Appl. Mater. Interfaces 2019, 11, 44521–44527.
- (15) Ebbens, S.; Hodgkinson, R.; Parnell, A. J.; Dunbar, A.; Martin, S. J.; Topham, P. D.; Clarke, N.; Howse, J. R. In Situ Imaging and Height Reconstruction of Phase Separation Processes in Polymer Blends during Spin Coating. *ACS Nano* **2011**, *5*, 5124–5131.
- (16) Müller-Buschbaum, P.; Gutmann, J. S.; Wolkenhauer, M.; Kraus, J.; Stamm, M.; Smilgies, D.; Petry, W. Solvent-Induced Surface Morphology of Thin Polymer Films. *Macromolecules*. **2001**, *34*, 1369–1375.
- (17) Strawhecker, K. E.; Kumar, S. K.; Douglas, J. F.; Karim, A. The Critical Role of Solvent Evaporation on the Roughness of Spin-Cast Polymer Films. *Macromolecules.* **2001**, *34*, 4669–4672.
- (18) Li, M.; Xu, S.; Kumacheva, E. Convection in Polymeric Fluids Subjected to Vertical Temperature Gradients. *Macromolecules.* **2000**, 33, 4972–4978.
- (19) Kim, J.-K.; Taki, K.; Nagamine, S.; Ohshima, M. Periodic Porous Stripe Patterning in a Polymer Blend Film Induced by Phase Separation during Spin-Casting. *Langmuir.* **2008**, *24*, 8898–8903.

- (20) Chiu, M.; Wood, J. A.; Widmer-Cooper, A.; Neto, C. Aligned Droplet Patterns by Dewetting of Polymer Bilayers. *Macromolecules*. **2018**, *51*, 5485–5493.
- (21) Wu, B.-H.; Chang, K.-C.; Hsu, H.-H.; Chiu, Y.-J.; Chiu, T.-Y.; Tseng, H.-F.; Li, J.-W.; Chen, J.-T. Radial Linear Polymer Patterns Driven by the Marangoni Instability and Lateral Phase Separation for the Formation of Nanoscale Perforation Lines. *ACS Appl. Nano Mater.* **2019**, *2*, 3253–3261.
- (22) Thickett, S. C.; Harris, A.; Neto, C. Interplay between Dewetting and Layer Inversion in Poly(4-Vinylpyridine)/Polystyrene Bilayers. *Langmuir* **2010**, *26*, 15989–15999.
- (23) Heriot, S. Y.; Jones, R. A. L. An Interfacial Instability in a Transient Wetting Layer Leads to Lateral Phase Separation in Thin Spin-Cast Polymer-Blend Films. *Nat. Mater.* **2005**, *4*, 782–786.
- (24) Tamai, Y.; Ohkita, H.; Benten, H.; Ito, S. Exciton Diffusion in Conjugated Polymers: From Fundamental Understanding to Improvement in Photovoltaic Conversion Efficiency. *J. Phys. Chem. Lett.* **2015**, *6*, 3417–3428.
- (25) Benten, H.; Mori, D.; Ohkita, H.; Ito, S. Recent Research Progress of Polymer Donor/Polymer Acceptor Blend Solar Cells. *J. Mater. Chem. A* **2016**, *4*, 5340–5365.
- (26) Kiesow, K. I.; Dhuey, S.; Habteyes, T. G. Mapping Near-Field Localization in Plasmonic Optical Nanoantennas with 10 nm Spatial Resolution. *Appl. Phys. Lett.* **2014**, *105*, 053105.
- (27) Li, J.; Jahng, J.; Pang, J.; Morrison, W.; Li, J.; Lee, E. S.; Xu, J.-J.; Chen, H.-Y.; Xia, X.-H. Tip-Enhanced Infrared Imaging with Sub-10 nm Resolution and Hypersensitivity. *J. Phys. Chem. Lett.* **2020**, *11*, 1697–1701.
- (28) Guo, X.; Facchetti, A. The Journey of Conducting Polymers from Discovery to Application. *Nat. Mater.* **2020**, *19*, 922–928.
- (29) Lee, C.; Lee, S.; Kim, G.-U.; Lee, W.; Kim, B. J. Recent Advances, Design Guidelines, and Prospects of All-Polymer Solar Cells. *Chem. Rev.* **2019**, *119*, 8028–8086.
- (30) Dąbczyński, P.; Pawłowska, A. I.; Majcher-Fitas, A. M.; Stefańczyk, O.; Dłubacz, A.; Tomczyk, W.; Marzec, M. M.; Bernasik, A.; Budkowski, A.; Rysz, J. Extraordinary Conduction Increase in Model Conjugated/Insulating Polymer System Induced by Surface Located Electric Dipoles. *Appl. Mater. Today.* **2020**, *21*, 100880.
- (31) Wang, C.-F.; Kafle, B.; Tesema, T. E.; Kookhaee, H.; Habteyes, T. G. Molecular Sensitivity of Near-Field Vibrational Infrared Imaging. *J. Phys. Chem. C* **2020**, *124*, 21018–21026.
- (32) Habteyes, T. G.; Dhuey, S.; Kiesow, K. I.; Vold, A. Probe-Sample Optical Interaction: Size and Wavelength Dependence in Localized Plasmon near-Field Imaging. *Opt. Express* **2013**, *21*, 21607–21617.
- (33) Habteyes, T. G. Direct Near-Field Observation of Orientation-Dependent Optical Response of Gold Nanorods. *J. Phys. Chem. C* **2014**, *118*, 9119–9127.
- (34) Ocelic, N.; Huber, A.; Hillenbrand, R. Pseudoheterodyne Detection for Background-Free Near-Field Spectroscopy. *Appl. Phys. Lett.* **2006**, *89*, 101124.
- (35) Goikoetxea, M.; Amenabar, I.; Chimenti, S.; Paulis, M.; Leiza, J. R.; Hillenbrand, R. Cross-Sectional Chemical Nanoimaging of Composite Polymer Nanoparticles by Infrared Nanospectroscopy. *Macromolecules.* **2021**, *54*, 995–1005.
- (36) Walheim, S.; Böltau, M.; Mlynek, J.; Krausch, G.; Steiner, U. Structure Formation via Polymer Demixing in Spin-Cast Films. *Macromolecules.* **1997**, *30*, 4995–5003.
- (37) Vukusic, P.; Sambles, J. R.; Lawrence, C. R. Structurally Assisted Blackness in Butterfly Scales. *Proc. Biol. Sci.* **2004**, 271, S237—S239.
- (38) Gao, Y.; Grey, J. K. Resonance Chemical Imaging of Polythiophene/Fullerene Photovoltaic Thin Films: Mapping Morphology-Dependent Aggregated and Unaggregated C=C Species. J. Am. Chem. Soc. 2009, 131, 9654–9662.
- (39) Shimizu, H.; Yamada, M.; Wada, R.; Okabe, M. Preparation and Characterization of Water Self-Dispersible Poly(3-Hexylthiophene) Particles. *Polym. J.* **2008**, *40*, 33–36.

- (40) Millstone, J. E.; Kavulak, D. F. J.; Woo, C. H.; Holcombe, T. W.; Westling, E. J.; Briseno, A. L.; Toney, M. F.; Fréchet, J. M. J. Synthesis, Properties, and Electronic Applications of Size-Controlled Poly(3-Hexylthiophene) Nanoparticles. *Langmuir* **2010**, *26*, 13056–13061.
- (41) Ma, H.; Dong, R.; Van Horn, J. D.; Hao, J. Spontaneous Formation of Radially Aligned Microchannels. *Chem. Commun.* **2011**, 47, 2047–2049.
- (42) Uchiyama, H.; Mantani, Y.; Kozuka, H. Spontaneous Formation of Linearly Arranged Microcraters on Sol-Gel-Derived Silica-Poly(vinylpyrrolidone) Hybrid Films Induced by Bénard-Marangoni Convection. *Langmuir* **2012**, *28*, 10177–10182.
- (43) Wu, K.-H.; Lu, S.-Y.; Chen, H.-L.; Chen, Y.-Y. Two-Dimensional Marangoni-Instability-Induced Periodic Patterns of Polymer Blend Films Cast on Tilted Substrates. *Macromol. Chem. Phys.* **2008**, 209, 615–624.
- (44) Hyun, W. J.; Im, S. H.; Ok Park, O.; Chin, B. D. Corrugated Structure through a Spin-Coating Process for Enhanced Light Extraction from Organic Light-Emitting Diodes. *Org. Electron.* **2012**, 13, 579–585.
- (45) Lu, S.-Y.; Chen, H.-L.; Wu, K.-H.; Chen, Y.-Y. Formation of Nanowire Striations Driven by Marangoni Instability in Spin-Cast Polymer Thin Films. *Langmuir* **2007**, 23, 10069–10073.
- (46) Agbolaghi, S.; Zenoozi, S. A Comprehensive Review on poly(3-Alkylthiophene)-Based Crystalline Structures, Protocols and Electronic Applications. *Org. Electron.* **2017**, *51*, 362–403.
- (47) Spano, F. C. Absorption in Regio-Regular Poly(3-Hexyl)-thiophene Thin Films: Fermi Resonances, Interband Coupling and Disorder. *Chem. Phys.* **2006**, 325, 22–35.
- (48) Brown, P. J.; Thomas, D. S.; Kohler, A.; Wilson, J. S.; Kim, J.-S.; Ramsdale, C. M.; Sirringhaus, H.; Friend, R. H. Effect of Interchain Interactions on the Absorption and Emission of Poly(3-Hexylthiophene). *Phys. Rev. B* **2003**, *67*, 064203.
- (49) Bates, F. S. Polymer-Polymer Phase Behavior. Science 1991, 251, 898-905.

□ Recommended by ACS

Highly Ordered Polymer Nanostructures via Solvent On-Film Annealing for Surface-Enhanced Raman Scattering

Kai-Jie Chang, Jiun-Tai Chen, et al.

DECEMBER 24, 2021

LANGMUIR

READ 🗹

Fabrication and Comparative Quantitative Analysis of Plasmonic-Polymer Nanocomposites as Optical Platforms

Casey Folks, Agampodi Swarnapali De Silva Indrasekara, et al.

OCTOBER 27, 2021

LANGMUIR

READ 🗹

A Quantitative Optical Microscopy Method for Investigating the Laser-Induced Transient Melting Behavior of a Nanoparticle-Laden Polymer System in...

Jingwen Yao, Tao Liu, et al.

JULY 30, 2020

THE JOURNAL OF PHYSICAL CHEMISTRY C

READ 🗹

Binary Nanoparticles Coassembly in Bioinspired Block Copolymer Films: A Stepwise Synthesis Approach Using Multifunctional Catechol Groups and Magneto-Optic...

Hideaki Komiyama, Hiroshi Yabu, et al.

MARCH 30, 2018

ACS APPLIED NANO MATERIALS

READ 🗹

Get More Suggestions >